Calculation of the electron momentum density in Zr and ZrH_2

N. I. Papanicolaou
Department of Physics, University of Ioannina, 453 32 Ioannina, Greece

N. C. Bacalis
Research Center of Crete, P.O. Box 1527, 71 110 Heraklion, Crete, Greece

D. A. Papaconstantopoulos
Naval Research Laboratory, Washington, D.C. 20375
(Received 19 June 1987)

The electron momentum distributions (EMD's) and two-photon momentum distributions (TPMD's) in Zr and ZrH_2 have been calculated by means of a self-consistent augmented-plane-wave method. The results of the calculation for the total EMD and TPMD in Zr and ZrH_2 along the [100], [110], and [111] directions, as well as the changes which appear on the introduction of hydrogen, can be understood on the basis of the respective energy bands and Fermi-surface topology. We also find the well-known feature that high-momentum components of the EMD have larger amplitudes than those of the corresponding TPMD.

I. INTRODUCTION

In recent years a growing number of measurements have been performed to study the electronic properties of solids by means of Compton scattering[1,2] or positron annihilation[3–5] techniques. The investigation of the momentum density in transition metals and metal-hydrogen systems[6] is of particular importance because of their interesting electronic structure and technological applications. In order to analyze the various experimental data, e.g., Compton profiles (CP's) or angular correlation of positron annihilation radiation (ACPAR), concerning these metals and compounds, we need a theoretical study of the electron momentum density employing an *ab initio* band-structure calculation.

Recently, an augmented-plane-wave (APW) band-structure calculation of the electron momentum distributions (EMD's) $\rho(\mathbf{p})$ and two-photon momentum distributions (TPMD's) $\rho_{2\gamma}(\mathbf{p})$ in Pd and stoichiometric PdH was reported.[7,8] It was shown that both EMD's and TPMD's change significantly in going from Pd to PdH. A self-consistent (SC) APW calculation of the CP's of Ti and TiH_2,[9] as well as of V, Nb, VH_2, and NbH_2,[10] has also been performed, showing remarkable differences between the respective CP's of the host metals and dihydrides.

Among other transition metals and hydrides, Zr and ZrH_2 have important technological applications in aircraft industry, nuclear reactors, etc. Zirconium crystallizes in the hcp structure and it is a 4*d* transition metal, which reacts with hydrogen to form the stoichiometric ZrH_2 in the cubic fluorite structure (CaF_2). Gupta and Loucks[11] calculated the angular dependence of the positron annihilation along the [001] direction in hcp zirconium. To our knowledge no theoretical or experimental data of EMD's or TPMD's exist in the case of ZrH_2.

We report here the results for EMD's and TPMD's in Zr (fcc) and ZrH_2 using the APW method, aiming to understand the relation between the changes in the $\rho(\mathbf{p})$ or $\rho_{2\gamma}(\mathbf{p})$ and the changes in the energy bands due to the formation of a dihydride. In the present work Zr was treated as a hypothetical fcc metal, in order to facilitate the comparison with its dihydride. In a previous paper[9] we showed that this approximation was reasonable in the case of the average CP of Ti, due to the fact that the two structures (fcc and hcp) have the same density. Our calculation was self-consistent and scalar-relativistic, using the Hedin-Lundqvist prescription for exchange and correlation.[12]

II. CALCULATION

The computation of the band structure for electrons and positrons has been performed self-consistently by means of the symmetrized augmented-plane-wave method[13] (SAPW) in the "soft-core" approximation as discussed elsewhere.[14] The calculation was scalar-relativistic, i.e., including Darwin and mass-velocity relativistic corrections, but neglecting spin-orbit coupling.[15] We used the local-density approximation of Hedin and Lundqvist[12] for the exchange and correlation part of the electron crystal potential, while there is no such term for the positron crystal potential. To calculate the positron wave function we used only the Coulomb part of the SC electron potential with opposite sign. To calculate the converged electron potentials we used a mesh of 20 k points in the $\frac{1}{48}$ part of the first Brillouin zone (BZ).

The lattice constants and muffin-tin (MT) sphere radii for the metal and the hydrogen atoms used in these calculations are listed in Table I. The converged electron crystal potentials were used to calculate eigenvalues and wave functions by the APW method on a mesh of 89 k points in the irreducible part of the first BZ.

The wave function $\Psi_j(\mathbf{k},\mathbf{r})$ of an electron in a state $\mathbf{k}$

TABLE I. Lattice constants (a) and muffin-tin sphere radii of the metal (R_M) and the hydrogen (R_H) in atomic units.

	Zr	ZrH_2
a	8.3155	9.0329
R_M	2.9399	2.5417
R_H		1.3682

and in the jth band is given by a linear combination of the APW functions $\psi(\mathbf{r},\mathbf{k}_i,j)$:[13]

$$\Psi_j(\mathbf{k},\mathbf{r})=\sum_i v(\mathbf{k}_i)\psi(\mathbf{r},\mathbf{k}_i,j), \quad \mathbf{k}_i=\mathbf{k}+\mathbf{G}_i \tag{1}$$

where $v(\mathbf{k}_i)$ are calculated eigenvectors from the APW secular determinant (with dimensions 70×70 for Zr and 90×90 for ZrH_2) and $\mathbf{G}_i$ are reciprocal lattice vectors around the center of the first BZ. The wave function ψ is a plane wave outside the MT spheres and follows a spherical harmonics expansion inside.

The positron wave function $\Psi_+(\mathbf{k},\mathbf{r})$ is calculated by the same expression (1). Because the positron is thermalized, or at $T=0$ in its ground state $\mathbf{K}_+=0$ with Γ_1 symmetry, its wave function can be approximated by only one term, $l=0$, inside the MT spheres.

We thus used:

$$\begin{aligned}\Psi_+(\mathbf{r})&=1 \quad \text{in the interstitial region ,}\\ &=u_+(|\mathbf{r}-\mathbf{r}_N|)/u_+(R_{\mathrm{MT}})\\ &\qquad\qquad \text{inside each MT sphere ,}\end{aligned} \tag{2}$$

where u_+'s are the radial positron wave functions at Γ_1.

The TPMD $\rho_{2\gamma}(\mathbf{p})$ can be expressed as

$$\rho_{2\gamma}(\mathbf{p})=\sum_{\substack{\mathbf{k},j\\ \text{occ.}}} |A_j(\mathbf{k},\mathbf{p})|^2 \tag{3}$$

where $A_j(\mathbf{k},\mathbf{p})$ is the Fourier transform of the product of electron and positron wave functions, i.e.,

$$A_j(\mathbf{k},\mathbf{p})=\delta(\mathbf{p}-\mathbf{k}-\mathbf{G})\int_{\mathrm{cell}}\exp(-i\mathbf{p}\cdot\mathbf{r})\Psi_j(\mathbf{k},\mathbf{r})\Psi_+(\mathbf{r})d\mathbf{r} . \tag{4}$$

The EMD $\rho(\mathbf{p})$ is obtained from (3) if $\Psi_+(\mathbf{r})$ is replaced by unity in expression (4).

Using Eqs. (1) and (2) for the wave functions in expression (4) we get $A_j(\mathbf{k},\mathbf{p})$:

$$A_j(\mathbf{k},\mathbf{p})=\delta(\mathbf{p}-\mathbf{k}-\mathbf{G})\sum_i v(\mathbf{k}_i)(\hat{\mathbf{f}}^{\mathrm{PW}}_{\mathbf{p},\mathbf{k}_i}+\hat{\mathbf{f}}^{\mathrm{IN}}_{\mathbf{p},\mathbf{k}_i}) \tag{5}$$

where the plane-wave term is,

$$\begin{aligned}\hat{\mathbf{f}}^{\mathrm{PW}}_{\mathbf{p}\cdot\mathbf{k}_i}=&\left[V_c-\sum_{\mathrm{MT}=1}^{N_A}V_{\mathrm{MT}}\right]\delta_{\mathbf{p},\mathbf{k}_i}\\ &-4\pi\sum_{\mathrm{MT}=1}^{N_A}(1-\delta_{\mathbf{p},\mathbf{k}_i})\\ &\times\exp[i(\mathbf{k}_i-\mathbf{p})\cdot\mathbf{r}_N]\\ &\times R^2_{\mathrm{MT}}\frac{j_l(|\mathbf{k}_i-\mathbf{p}|R_{\mathrm{MT}})}{|\mathbf{k}_i-\mathbf{p}|} ,\end{aligned} \tag{6}$$

with V_c and V_{MT} the volume of the unit cell and of each MT sphere respectively, and the interstitial term is

$$\begin{aligned}\hat{\mathbf{f}}^{\mathrm{IN}}_{\mathbf{p},\mathbf{k}_i}=&4\pi\sum_{\mathrm{MT}=1}^{N_A}\exp[i(\mathbf{k}_i-\mathbf{p})\cdot\mathbf{r}_N]\sum_{l=0}^{l_{\max}}(2l+1)J_l(k_iR_{\mathrm{MT}})P_l[\mathbf{p}\cdot\mathbf{k}_i/(pk_i)]\\ &\times\int_0^{R_{\mathrm{MT}}}r^2u_l(r,j)u_+(r)j_l(pr)dr/[u_l(R_{\mathrm{MT}},j)u_+(R_{\mathrm{MT}})] ,\end{aligned} \tag{7}$$

with P_l's the Legendre polynomials. For each $\mathbf{k}$, the expression $A_j(\mathbf{k},\mathbf{p})$ is normalized as

$$\sum_{\mathbf{G}}|A_j(\mathbf{k},\mathbf{p})|^2=1 . \tag{8}$$

We have used 181 reciprocal lattice vectors G in momentum space. Equations (1)–(8) are the basis for our calculations of EMD $\rho(\mathbf{p})$ and TPMD $\rho_{2\gamma}(\mathbf{p})$ in Zr and its dihydride.

III. RESULTS AND DISCUSSION

A. Band structure

The calculated densities of states (DOS's) and energy bands of Zr (fcc) and ZrH_2 along some important symmetry directions are plotted in Figs. 1 and 2, respectively. The dashed horizontal line represents the Fermi energy E_F.

Table II shows a comparison of the calculated band en-

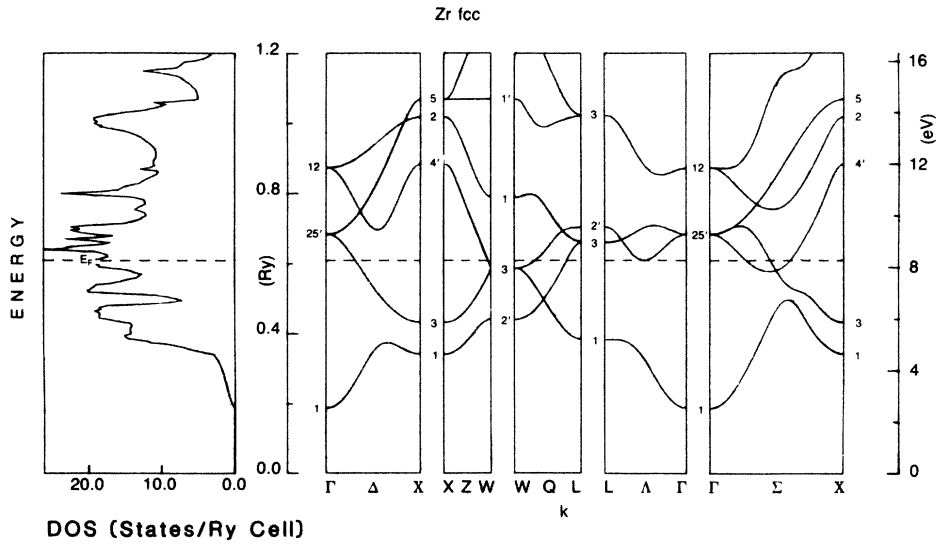

FIG. 1. The density of states and energy bands of Zr (fcc) along high-symmetry directions.

ergies (in Ry) of Zr by Moruzzi *et al.*[16] with the present results. They find $N(E_F)=17.42$ states/Ry atom for the DOS at E_F, while our calculation gives 18.53 states/Ry atom. In their work they employed the nonrelativistic self-consistent Korringa-Kohn-Rostocker (KKR) method in the muffin-tin approximation with the exchange and correlation of Hedin-Lundqvist. The small discrepancies between the present eigenvalues and the reported data of Morruzzi *et al.*[16] are due to the different methods used to solve the one-electron problem and to the fact that we have included relativistic effects. It is well known[14] that in the relativistic calculations the bands become wider and deeper in energy; From Table II we see that the most affected energy is that of the *s*-like Γ_1 state (about 40 mRy difference), while the *d* states are affected the least.

The band structure of ZrH_2 has been extensively discussed by Gupta,[17] Switendick,[18] and Papaconstantopoulos and Switendick.[19] As far as the band structure is concerned we note that there is no difference between the method and the approximations used in the latter paper[19] and the present work, therefore we will point out only the essential features of its electronic structure necessary for the present discussion.

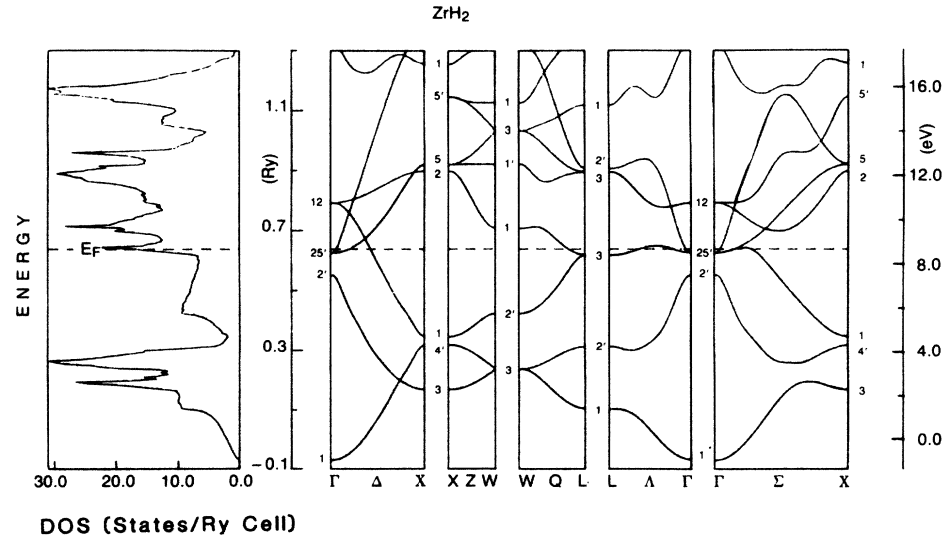

FIG. 2. The density of states and energy bands of ZrH_2 along high-symmetry directions.

TABLE II. Comparison of eigenvalues (in Ry) for some high-symmetry points in the Brillouin zone of zirconium between this work and that of Moruzzi *et al.*

Symmetry point	MJW[a] E (Ry)	Present results E (Ry)
Γ_1	0.224	0.187
$\Gamma_{25'}$	0.665	0.682
X_1	0.337	0.341
X_3	0.420	0.431
L_1	0.389	0.383
L_3	0.643	0.659
$L_{2'}$	0.713	0.702
$W_{2'}$	0.435	0.441
W_3	0.579	0.586
K_1	0.410	0.416
K_1	0.494	0.501
K_3	0.697	0.700

[a]Reference 16.

At low energies we observe two energy bands (Fig. 2). The first lower band represents metal-hydrogen bonding states corresponding to the first band of the pure metal; these states lie lower in energy than in the host metal due to the introduction of hydrogen. The second low-lying band involves mainly hydrogen-hydrogen and a weak metal-hydrogen interaction and overlaps the d states of metal located at higher energies; the $\Gamma_{2'}$ level (hydrogen-hydrogen antibonding states) lies below the Fermi energy E_F. In addition we note the presence of the two sharp peaks in the DOS at low energies, which are characteristic of the metal-hydrogen bonding interaction.

B. Electron momentum distribution

The calculated total EMD $\rho(\mathbf{p})$ in Zr along the symmetry directions [100], [110], and [111] are plotted in Fig. 3. The insets show the corresponding energy bands.

Harthoorn and Mijnarends[20] have discussed a selection rule which allows only certain bands to contribute to the total $\rho(\mathbf{p})$, while the partial momentum distributions of the other bands are zero. According to this rule, only the bands Δ_1, Σ_1 and Λ_1 (the totally symmetric representations) are allowed to contribute to $\rho(\mathbf{p})$ in the first and higher Brillouin zones along the [100], [110], and [111] directions, respectively. The labels (A), (B), etc. marked in the band structure (inset) of Fig. 3 show the lower and higher Δ_1, Σ_1, and Λ_1 bands, respectively. It should be noted here that in our calculation we have verified the

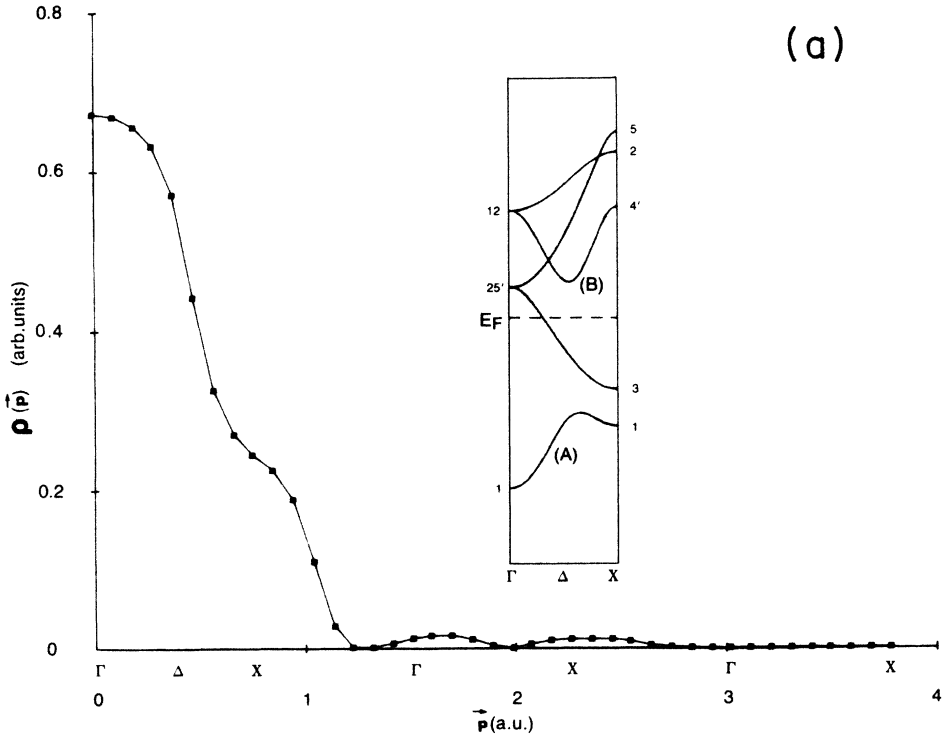

FIG. 3. The calculated EMD $\rho(\mathbf{p})$ due to the band electrons of Zr (fcc) along (a) [100], (b) [110], and (c) [111] directions. (The solid lines connect the computed points.) The corresponding energy bands are shown in the inset.

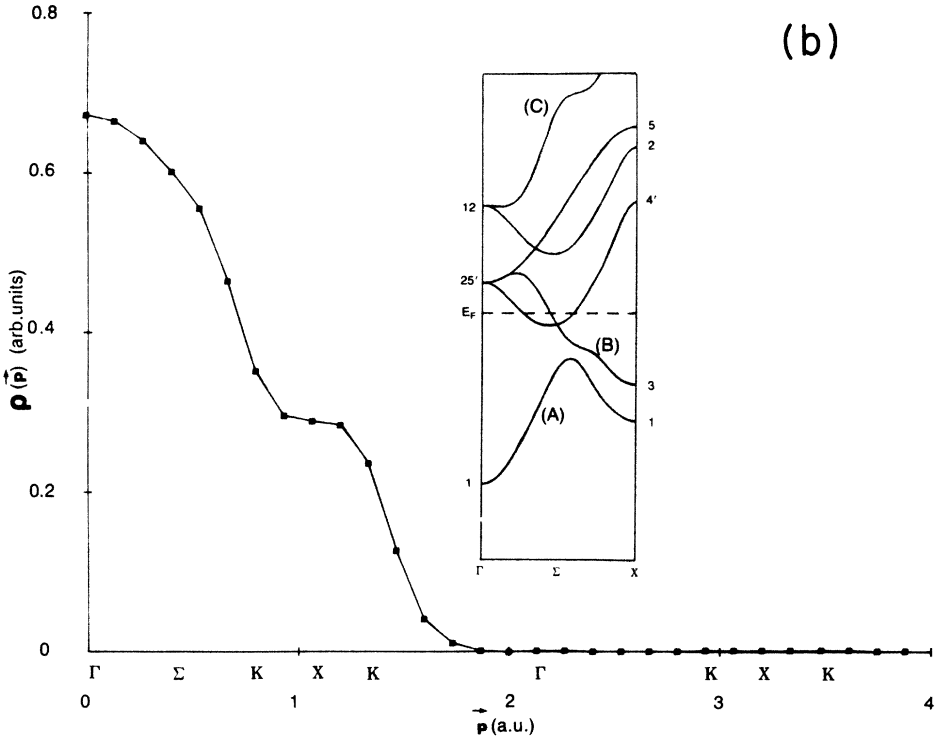

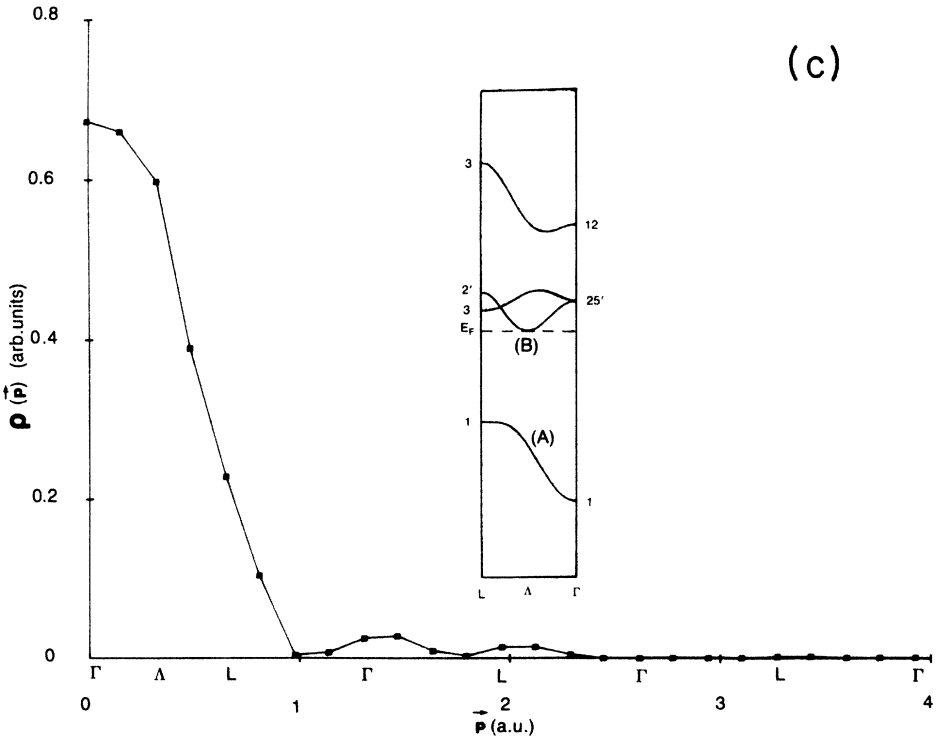

FIG. 3. (*Continued*).

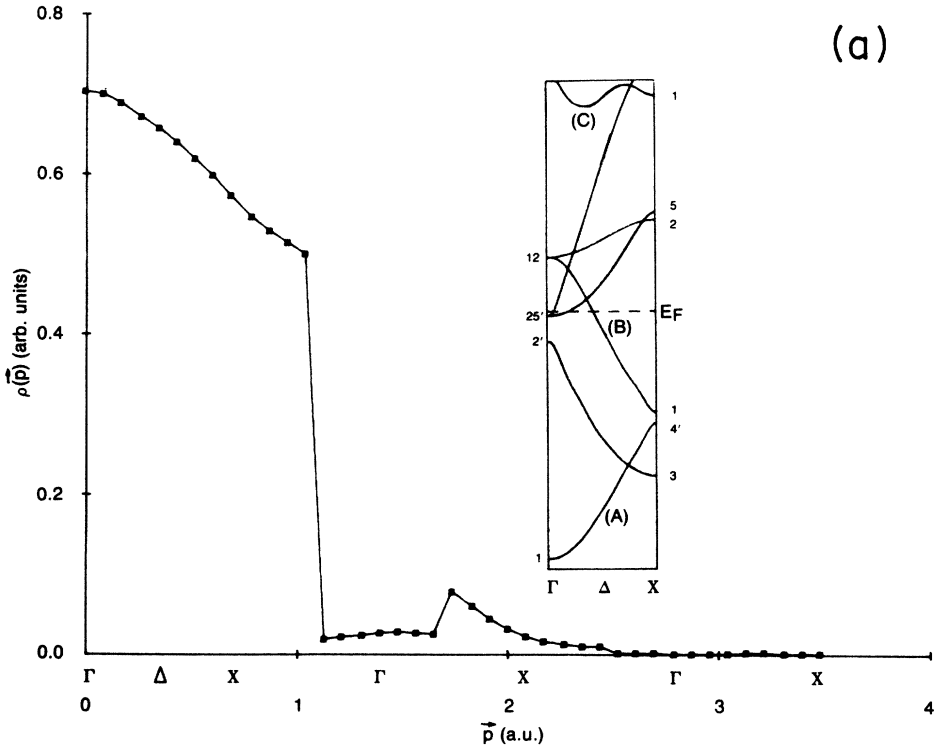

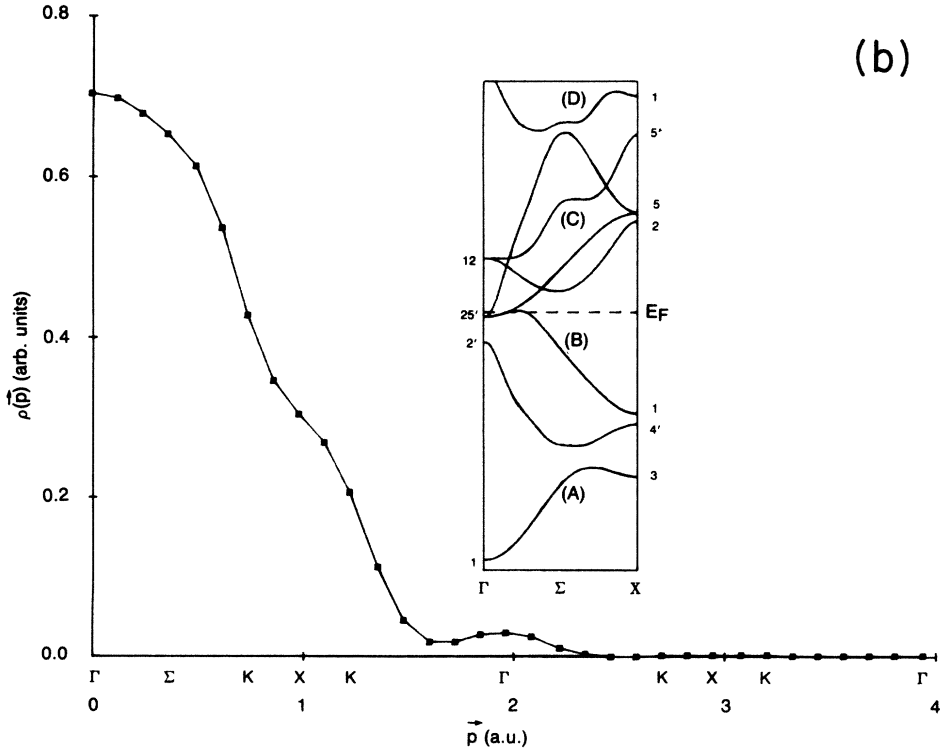

FIG. 4. The same as Fig. 3 but for ZrH_2.

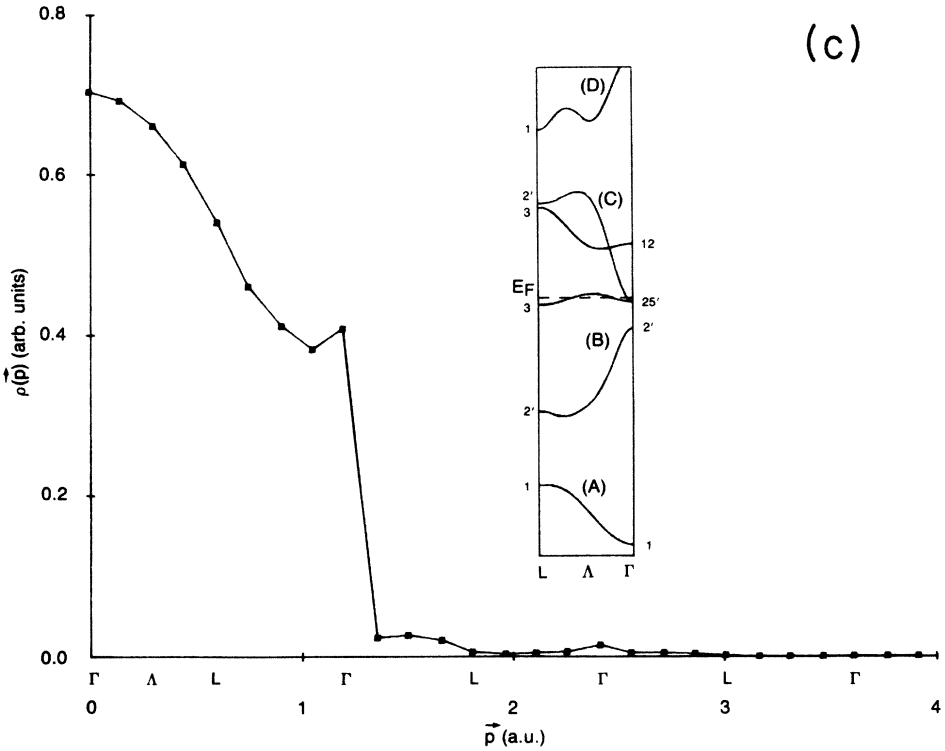

FIG. 4. (*Continued*).

above selection rule: The other bands give a contribution only $10^{-14}\%$ of the total $\rho(\mathbf{p})$, which is at the limit of detection.

The effects of the band structure, character of wave functions and Fermi-Surface topology on the EMD in $3d$ and $4d$ transition metals have been reported by several authors.[21–26] Here we will discuss in a similar manner our theoretical results of $\rho(\mathbf{p})$ in Zr.

Along the [100] direction [Fig. 3(a)] only the lowest Δ_1, band is occupied (labeled by A). Thus the total EMD is due only to the contribution of one completely occupied band; since the Fermi level lies well above this band, the $\rho(\mathbf{p})$ has a smooth shape inside the first BZ ($\mathbf{G}=0$) without discontinuities. At low momenta the behavior of $\rho(\mathbf{p})$ is almost flat due to the s-like character of the Γ_1 state. When p increases, the momentum distribution begins to decrease, since this Δ_1 band loses its s character owing to hydridization with the d band; the X_1 level has predominantly a d like character. The presence of the high-momentum components (HMC) of the $\rho(\mathbf{p})$ in the higher zones is due to the Umklapp process $\mathbf{p}=\mathbf{k}+\mathbf{G}$ ($\mathbf{G}\neq\mathbf{0}$) while their amplitude is determined by the value of the term $|A_j(\mathbf{k},\mathbf{p})|^2$.

In the case of the EMD along the [110] direction [Fig. 3(b)] the behavior of the lowest Σ_1 band [marked A] is similar to that of the lowest Δ_1 band. The next higher Σ_1 band (marked B) is partially occupied; it starts at $\Gamma_{25'}$ as a d band, since the $\Gamma_{25'}$ level is a pure d state and it remains d-like inside the first BZ. At low p the partial momentum density of this band increases slowly as p^4,[22,27] but there is no contribution to the total $\rho(\mathbf{p})$, because it is not occupied. At $p\sim 0.5$ a.u. this band crosses the Fermi level and starts contributing to the total EMD. As it is expected,[25,27] no visible Fermi discontinuity occurs at this momentum because the contribution of this d-like band is small there. The contribution of the latter is predominant in the second BZ and it gives a broadening of the total $\rho(\mathbf{p})$. In the region $1.7<p<2.6$ a.u. (on either side of Γ) the HMC's of the $\rho(\mathbf{p})$ given by the upper Σ_1 band (B) are absent, since the corresponding states lie above the Fermi level.

Concerning the EMD along the [111] direction [Fig. 3(c)] the behavior of the lowest Λ_1 band (labeled by A) can be analyzed similarly to the lowest Δ_1 band. The upper Λ_1 band (marked B) lies close to the Fermi energy but fails to contribute to the total $\rho(\mathbf{p})$ because it is not occupied throughout. Thus the shape of $\rho(\mathbf{p})$ along this symmetry direction is determined by the contribution of only one completely occupied Λ_1 band.

In Fig. 4 we show the $\rho(\mathbf{p})$ of ZrH_2 along the high symmetry directions Δ, Σ, and Λ. The respective energy bands are plotted in the inset. It is clear that the introduction of hydrogen results in quite different EMD's from those of the pure metal. These differences can be understood in terms of the changes in the energy bands along with the changes in the character of the respective wave functions.

Along the symmetry directions Δ, Σ, and Λ the lower

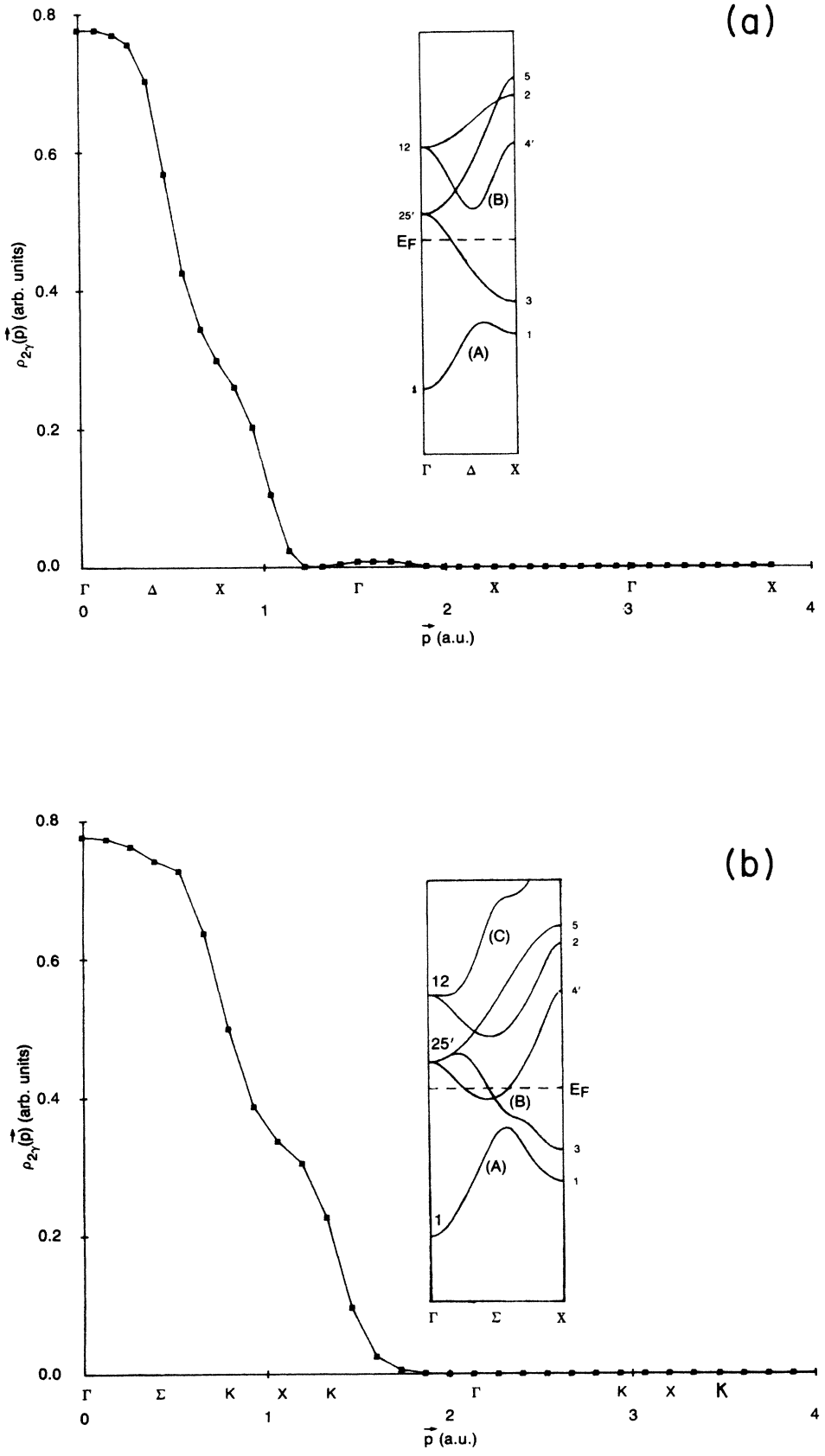

FIG. 5. The TPMD $\rho_{2\gamma}(\mathbf{p})$ for the band electrons in Zr (fcc) along (a) [100], (b) [110], and (c) [111] directions. (The solid lines connect the calculated points.) The insets show the relevant energy bands.

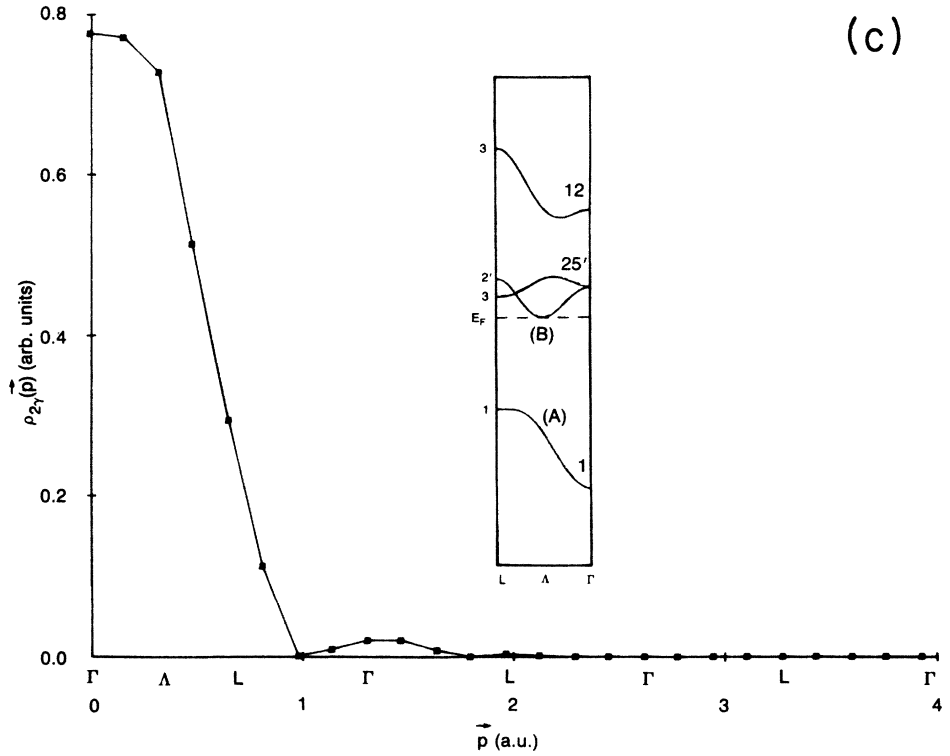

FIG. 5. (*Continued*).

bands Δ_1, Σ_1 and Λ_1 [marked as *A* in Figs. 4(a)–4(c), respectively) are formed from metal-hydrogen bonding states. At Γ_1 these bands are obtained by a bonding combination of zirconium 5*s* and hydrogen 1*s* states. As *p* increases, contributions of other states of the metal (*p* or *d*-like states) appear, but these remain small compared with the contribution of the *s*-like H states; the partial EMD's due to these low-lying bands begin to decrease slowly and involve generally small values in higher zones. They are also broader in ZrH_2 than in Zr, since the corresponding states lie lower in energy than in the pure metal; a lowering of the energy means being closer to the nucleus and hence having higher average momenta.[7]

As is shown in Fig. 4(a), the next higher Δ_1 band (marked *B*) is partially occupied and causes interesting features in the $\rho(\mathbf{p})$ along the [100] direction. This band has essentially a *d*-like character (due to Zr *d* states); thus the Fermi discontinuity is negligible inside the first BZ, when the band crosses the Fermi level. On the contrary, a strong Fermi break occurs at the equivalent momentum $p \sim 1.1$ a.u. through the Umklapp process. In the range $p = 1.1-1.7$ a.u. the $\rho(\mathbf{p})$ results only from the contribution of the lower Δ_1 band. Beyond $p \sim 1.7$ a.u. the upper Δ_1 band also yields nonzero contributions and we observe another weaker Fermi discontinuity at this momentum. A comparison of the total $\rho(\mathbf{p})$ for Zr along the Δ direction [Fig. 3(a)] with that of ZrH_2 [Fig. 4(a)] shows that the latter is broader and it presents discontinuities due to the additional contribution of the partially occupied upper Δ_1 band.

Similarly the next higher Σ_1 band [labeled by *B* in Fig. 4(b)] is formed mainly of *d*-like Zr states, but now it is almost completely occupied throughout the BZ; thus it gives a rather smooth partial contribution to the total $\rho(\mathbf{p})$. The minimum at $p \sim 1.7$ a.u. corresponds to the unoccupied part of the Σ_1 band in the second BZ. The total EMD along the Σ direction has generally similar shape in Zr and ZrH_2 [Figs. 3(b) and 4(b), respectively] except for the presence of the HMC of $\rho(\mathbf{p})$ for ZrH_2 around $p = 2$ a.u. The absence of the latter in Zr is attributed to the fact that the upper Σ_1 band in the host metal is partially occupied.

Along the [111] direction [Fig. 4(c)] the next higher Λ_1 band (marked as *B*) is completely occupied; it starts at $\Gamma_{2'}$ level, which is formed of hydrogen-hydrogen antibonding combination (*s*-like character) with a small *f*-like Zr contribution, but it does not give a visible contribution to $\rho(\mathbf{p})$.[20] As *p* increases the H-H antibonding states hybridize with mainly the Zr *p*-like states and the partial contribution of this band increases up to 0.9 a.u. and then decreases showing a smooth behavior. Up to $p = 1.2$ a.u. the contribution of this Λ_1 band gives a broader $\rho(\mathbf{p})$ compared with that for Zr [Fig. 3(c)]. In addition there is a higher Λ_1 band (marked *C*), which is occupied only near the center of the BZ and starts at $\Gamma_{25'}$ with an essentially *d*-like Zr character. At $p = 0$ it fails to give a visible contribution, but at $p = 1.2$ and 2.4 a.u. the observed peaks on the total $\rho(\mathbf{p})$ are due to the partial

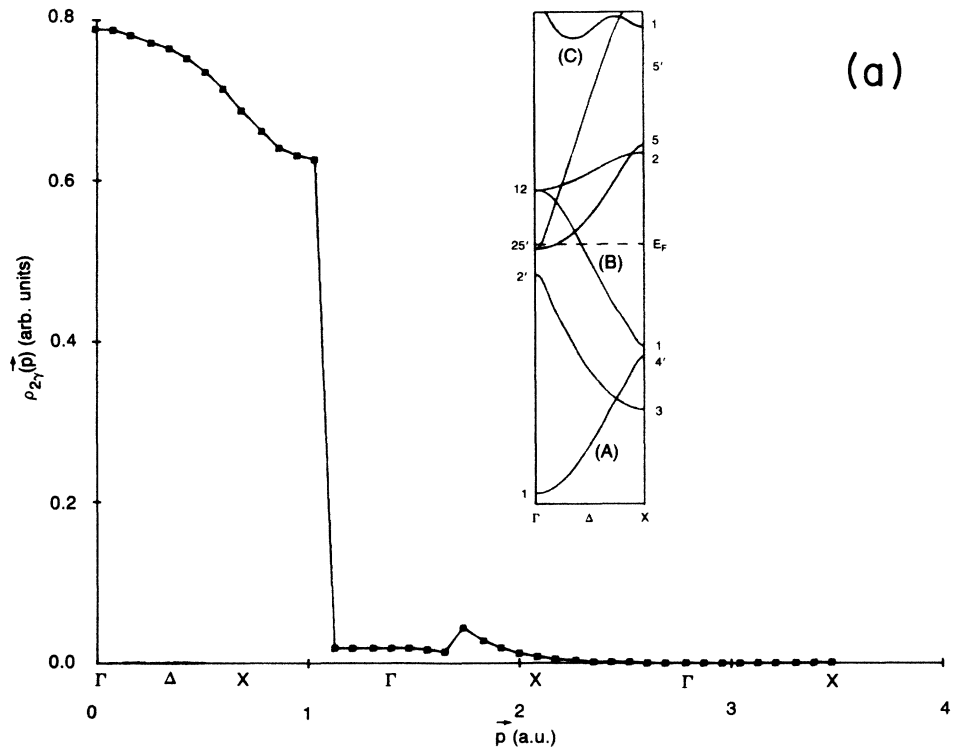

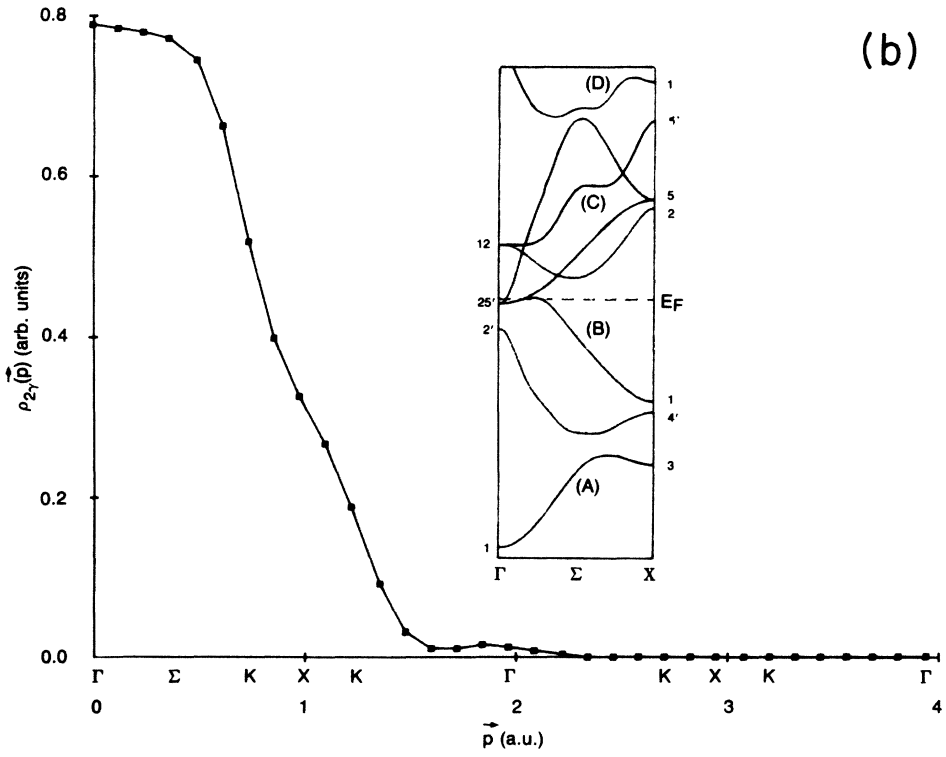

FIG. 6. The same as Fig. 5 but for ZrH_2.

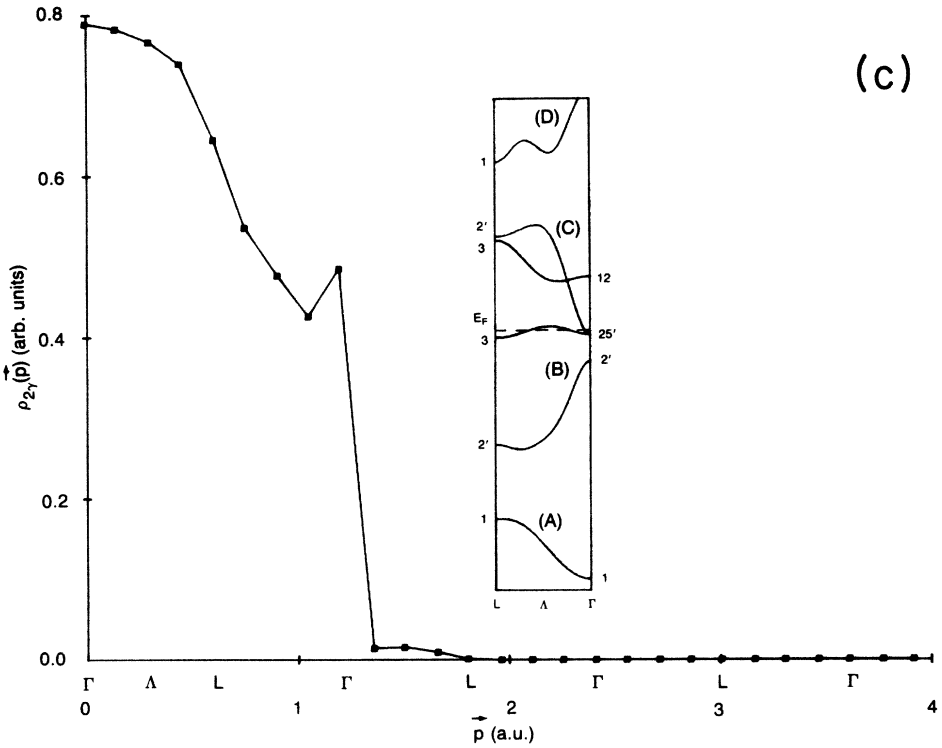

FIG. 6. (*Continued*).

contribution of the $\Gamma_{25'}$ state through the Umklapp process. A sharp Fermi break is shown at $p \sim 1.3$ a.u. arising from the crossing of the latter band with the Fermi level.

C. Two-photon momentum distribution

The calculated total TPMD's $\rho_{2\gamma}(\mathbf{p})$ along the three symmetry directions [100], [110], and [111] for Zr and ZrH_2 are presented in Figs. 5 and 6, respectively. A direct comparison of the above curves with those of the EMD's in Figs. 3 and 4 shows that the general shape as well as the various features and discontinuities of the corresponding curves are very similar for both metal and dihydride, so they can be interpreted in a manner similar to the one used previously. Nevertheless some differences do exist. For instance, the HMC's of the TPMD have smaller heights than those of the respective EMD. This is obviously a result of the presence of the positron wave function which reduces the contribution of the core orbitals in $\rho_{2\gamma}(\mathbf{p})$.[22]

It should also be pointed out that the Fermi breaks which occur in ZrH_2 at $p \sim 1.1$ and 1.3 a.u. along the [100] and [111] directions, respectively, are sharper for the TPMD (Fig. 6) than for the EMD (Fig. 4). An analogous difference between $\rho(\mathbf{p})$ and $\rho_{2\gamma}(\mathbf{p})$ has been found in Pd and PdH,[7,8] and reflects the presence of the positron wave function in the calculation of each partial contribution to the total TPMD.

IV. CONCLUSION

We have presented a calculation of EMD's and TPMD's in Zr and ZrH_2 using the self-consistent APW method. The behavior of $\rho(\mathbf{p})$ and $\rho_{2\gamma}(\mathbf{p})$ for the host metal and the dihydride along the symmetry directions Δ, Σ, and Λ, as well as the remarkable differences which occur on the momentum density upon the introduction of hydrogen are interpreted in terms of the respective energy bands, the Fermi-surface topology, and the character of the wave functions.

To our knowledge this is the first *ab initio* calculation of the changes involved in the EMD's and TPMD's of a 4*d* transition metal upon the formation of its dihydride. Unfortunately no experimental data like Compton profiles or angular correlation of positron annihilation radiation are available in the case of Zr and ZrH_2 for comparison with the present theoretical results. It is hoped that the above calculations will stimulate experimentalists to perform measurements on this metal and dihydride.

ACKNOWLEDGMENT

These calculations were performed at the Research Center of Crete.

[1]*Compton Scattering,* edited by B. Williams (McGraw-Hill, New York, 1977).
[2]M. J. Cooper, Rep. Prog. Phys. **48**, 415 (1985).
[3]*Positron in Solids,* edited by P. Hautojärvi (Springer, Berlin, 1979).
[4]*Positron Solid-State Physics,* edited by W. Brandt and A. Dupasquier (North-Holland, Amsterdam, 1983).
[5]*Positron Annihilation,* edited by P. C. Jain, R. M. Singru, and K. P. Gopinathan (World-Scientific, Singapore, 1985).
[6]*Hydrogen in Metals,* edited by G. Alefeld and J. Völkl (Springer, Berlin, 1978), Vols. I and II.
[7]A. Harmalkar, D. G. Kanhere, and R. M. Singru, Phys. Rev. B **31**, 6415 (1985).
[8]A. Kshirsagar, D. G. Kanhere, and R. M. Singru, Phys. Rev. B **34**, 853 (1986).
[9]N. C. Bacalis, N. I. Papanicolaou, and D. A. Papaconstantopoulos, J. Phys. F **16**, 1471 (1986).
[10]N. I. Papanicolaou, N. C. Bacalis, and D. A. Papaconstantopoulos, Z. Phys. B **65**, 453 (1987).
[11]R. P. Gupta and T. L. Loucks, Phys. Rev. **176**, 848 (1968).
[12]L. Hedin and B. I. Lundqvist, J. Phys. C **4**, 2064 (1971).
[13]L. F. Mattheiss, J. H. Wood, and A. C. Switendick, Methods Comput. Phys. **8**, 63 (1968).
[14]N. C. Bacalis, K. Blathras, P. Thomaides, and D. A. Papaconstantopoulos, Phys. Rev. B **32**, 4849 (1985).
[15]D. D. Koelling and B. N. Harmon, J. Phys. C **10**, 3107 (1977).
[16]V. L. Moruzzi, J. F. Janak, and A. R. Williams, *Calculated Electronic Properties of Metals* (Pergamon, New York, 1978), p. 120.
[17]M. Gupta, Phys. Rev. B **25**, 1027 (1982).
[18]A. C. Switendick, J. Less-Common. Met. **101**, 191 (1984).
[19]D. A. Papaconstantopoulos and A. C. Switendick, J. Less-Common Met. **103**, 317 (1984).
[20]R. Harthoorn and P. E. Mijnarends, J. Phys. F **8**, 1147 (1978).
[21]P. E. Mijnarends, Physica (Utrecht) **63**, 235 (1973).
[22]R. M. Singru and P. E. Mijnarends, Phys. Rev. B **9**, 2372 (1974).
[23]D. G. Kanhere and R. M. Singru, J. Phys. F **7**, 2603 (1977).
[24]R. Podloucky, R. Lässer, E. Wimmer, and P. Weinberger, Phys. Rev. B **19**, 4999 (1979).
[25]D. G. Kanhere, R. M. Singru, and R. Harthoorn, Phys. Status Solidi B **105**, 715 (1981).
[26]S. B. Shrivastava and V. K. Ojha, Phys. Status Solidi B **121**, 225 (1984).
[27]P. E. Mijnarends, in *Positron Solid-State Physics,* edited by W. Brandt and A. Dupasquier (North-Holland, Amsterdam, 1983), p. 146.